Simulations of the Flow in Supersonic Turbines with Straight Centerline Nozzles

Daniel J. Dorney*
Virginia Commonwealth University, Richmond, Virginia 23284-3015
Lisa W. Griffin†
NASA Marshall Space Flight Center, Huntsville, Alabama 35812
and
Karen L. Gundy-Burlet‡
NASA Ames Research Center, Moffett Field, California 94035

Introduction

FLOW unsteadiness is a major factor in turbine performance and durability. This is especially true if the turbine is a high-work design, compact, transonic, supersonic, counter rotating, or uses a dense drive gas. The vast majority of modern rocket turbine designs fall into these categories. For example, the Space Transportation System main engine fuel turbine, a high-work, transonic design, was found to have an unsteady interrow shock that reduced efficiency by 2 points and increased dynamic loading by 24% (Ref. 1). The revolutionary reusable technology turbopump (RRTT), which uses full-flow oxygen for its drive gas, was found to shed vortices with such energy as to raise serious blade durability concerns.[2] In both cases, the sources of the problems were uncovered (before turbopump testing) with the application of validated, unsteady computational fluid dynamics (CFD) to the designs. In the case of the RRTT and the alternate turbopump development turbines, the unsteady CFD codes have been used not just to identify problems, but to guide designs that mitigate problems due to unsteadiness.

As requirements for smaller and lighter weight components push turbines to more compact, closely coupled designs, flow unsteadiness increases. Current designs such as the Fastrac and future designs like the reusable launch vehicle fuel turbine add the complexities of supersonic flow regimes. The ability to predict accurately this flow unsteadiness in a timely manner is crucial to producing a design that meets program objectives. In this study, three different methods of applying unsteady three-dimensional Navier–Stokes analyses to the Fastrac nozzle/supersonic turbine geometry have been studied.

Governing Equations and Modeling Approximations

The governing equations considered are the time-dependent, three-dimensional Reynolds-averaged Navier–Stokes equations. The numerical algorithm used in the three-dimensional computational procedure consists of a time-marching, implicit, finite difference scheme. The procedure is third-order spatially accurate and second-order temporally accurate. The inviscid fluxes are discretized according to the scheme developed by Roe.[3] The viscous fluxes are calculated using standard central differences. An approximate-factorization technique is used to compute the time rate changes in the primary variables. In addition, Newton subiterations are used at each global time step to increase stability and to reduce linearization errors. For all cases investigated, two Newton subiterations were performed at each time step. Further details on the numerical procedure can be found in Refs. 4 and 5.

Three different modeling approximations have been studied:

1) In the turbine alone (TA) technique, the average flow quantities upstream of the turbine are obtained from a simulation of the nozzle in isolation. The endwalls at the turbine inlet are adjusted to provide the proper amount of mass flow. This is currently the standard technique for predicting the flow in nozzle/turbine geometries.

2) In the uncoupled simulation (UN) technique, the average flow quantities at the exit of the nozzle, including the solid portions of the nozzle ring, are modeled as part of inlet boundary conditions. As with the TA technique, the nozzle simulation is performed independently of the turbine simulation. The advantage of the UN technique is that the flow stagnation regions associated with the nozzle ring/turbine junctures are modeled.

3) In the coupled simulation (CO) technique, the nozzle and turbine flowfields are solved simultaneously, with the appropriate transfer of flow variable information.

Geometry and Grid

The actual supersonic turbine configuration consists of 24 nozzles, 147 rotor airfoils, and 67 exit guide vane (EGV) airfoils. In the TA and UN simulations, a one-nozzle/two-rotors/one-EGV blade count approximation is made. To keep the pitch-to-chord ratios constant, the rotor blades were scaled by a factor of $\frac{147}{150}$, and the EGVs were scaled by a factor of $\frac{67}{75}$. This scaling also assumes that the nozzles are a continuous slit around the annulus. The TA and UN simulations utilized 51 spanwise planes and contained a total of 818,358 grid points. The average value of y^+, the nondimensional distance of the first grid line above the surface, was approximately 1.0 for the airfoils surfaces and 1.5 for the endwall surfaces.

The nozzle was discretized using an O grid with a collapsing line at the centerline. The grid contained 108 points in the axial direction, 38 points in the circumferential direction, and 31 points in the region from the centerline to the outer wall. Thus, a total of 127,224 points were used to discretize the nozzle.

In the CO simulation, a one-nozzle/six-rotors/three-EGVs blade count approximation was made. To keep the pitch-to-chord ratios constant, the rotor blades were again scaled by a factor of $\frac{147}{150}$, and the EGV airfoils were again scaled by a factor of $\frac{67}{75}$. This blade count, however, correctly represents the presence of one nozzle. The CO simulation utilized 41 spanwise planes and contained a total of 1,545,987 grid points (see Fig. 1). Note that the computational grid density at each spanwise plane was the same as in the TA and UN simulations. The average value of y^+, the nondimensional distance of the first grid line above the surface, was approximately 1.0 for the

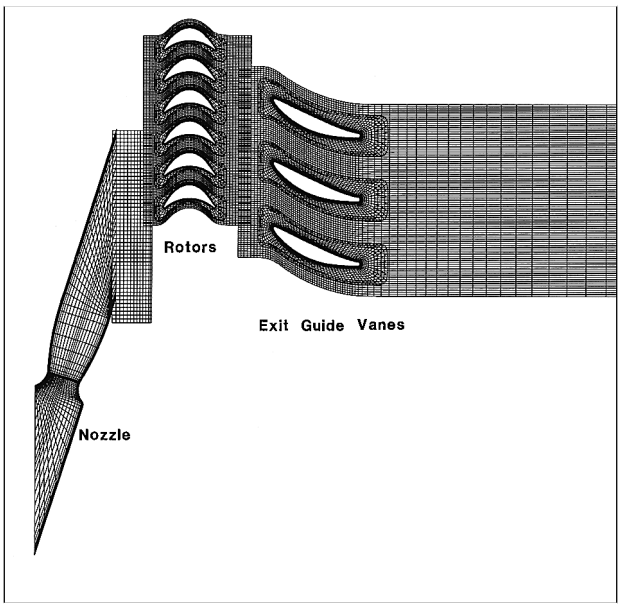

Fig. 1 Computational grid for the nozzle/turbine geometry.

Received 28 December 1998; revision received 4 September 1999; accepted for publication 29 September 1999.

*Associate Professor, Department of Mechanical Engineering. Senior Member AIAA.
†Team Leader, Fluid Dynamics Analysis Branch.
‡Acting Deputy Branch Chief, Computational Physics and Simulations Branch.

airfoils surfaces and 4.0 for the endwall surfaces. Figure 2 shows the topology at the interface of the nozzle exit and the rotor inlet.

Numerical Results, Time-Averaged and Unsteady Pressures

The Fastrac nozzle was designed to have an inlet Mach number of $M_0 \approx 0.23$ and an exit Mach number of $M_1 \approx 2.13$. The nozzle inlet static temperature is 889 K, and the ratio of specific heats is $\gamma = 1.108$. The turbine rotates at $\Omega = 20{,}000$ rpm. The Reynolds number was set at $Re = 1 \times 10^6$ based on the nozzle inlet conditions and the rotor axial chord. The working fluid is RP1 rocket fuel.

Figure 3 contains the time-averaged pressure distributions at the midspan section of the rotor. The TA and UN simulation yield similar time-averaged pressure distributions, including an even loading distribution. The CO simulation produces significantly more loading near the leading edge of the rotor. The aft portion of the rotor in the CO simulation tends to unload because of a suction surface separation bubble, which is much larger than in the TA and UN simulations. The separation bubble exhibits large temporal variations as the rotors move in and out of the wakes generated by the nozzle (see Fig. 4). Note that modeling of the nozzle in the UN simulation drives the solution closer to the CO results than the TA simulation.

The importance of coupling the nozzle and turbine simulations is demonstrated in Fig. 5, which shows a Fourier decomposition of the unsteady pressure at the point where the nozzle wake impacts the rotor in the lower half-span of the blade. The nozzle passing frequency is about 8000 Hz, whereas the blade passing frequency is approximately 48,000 Hz, that is, there are six rotors for each nozzle. The CO simulation indicates large levels of unsteadiness at frequencies between the nozzle and blade passing frequencies, which is consistent with the expected behavior because of the gap between the nozzles and rotors. The UN simulation appears to significantly underpredict the interaction (unsteadiness) of the nozzle and rotor blades.

The radial distribution of the circumferentially averaged Mach number at the rotor inlet is shown in Fig. 6. The CO simulation displays the thickest endwall boundary layers, followed by the UN simulation. The impingement of the nozzle jet in the tip endwall region is evident in the CO simulation, whereas the distribution in UN simulation is nearly symmetric about midspan. The boundary layers in the TA simulation are very thin. All three simulations produce midspan Mach numbers of approximately $M_2 = 2.10$. Note that the mass flow was the same in all three simulations; the hub

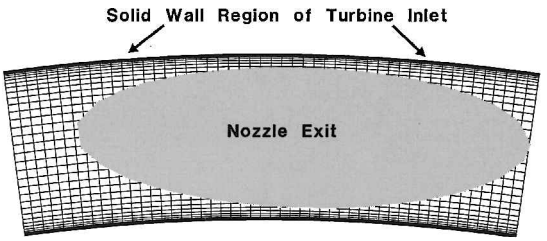

Fig. 2 Axial direction view of the nozzle exit/rotor inlet interface.

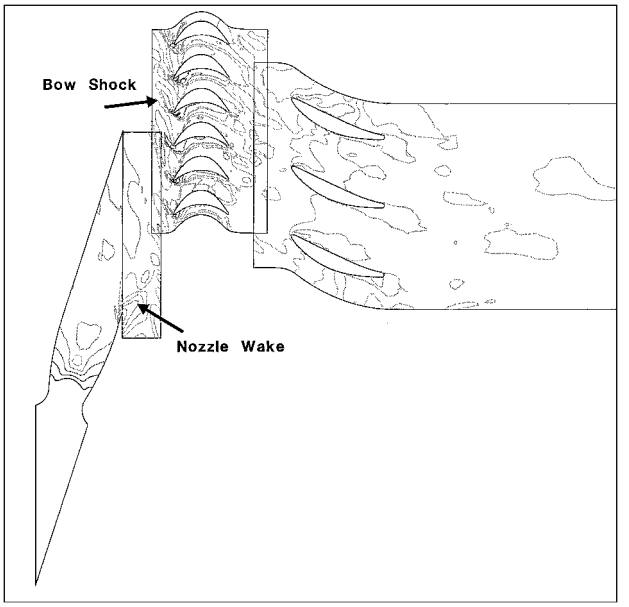

Fig. 4 Instantaneous entropy contours for midspan of the nozzle/turbine geometry.

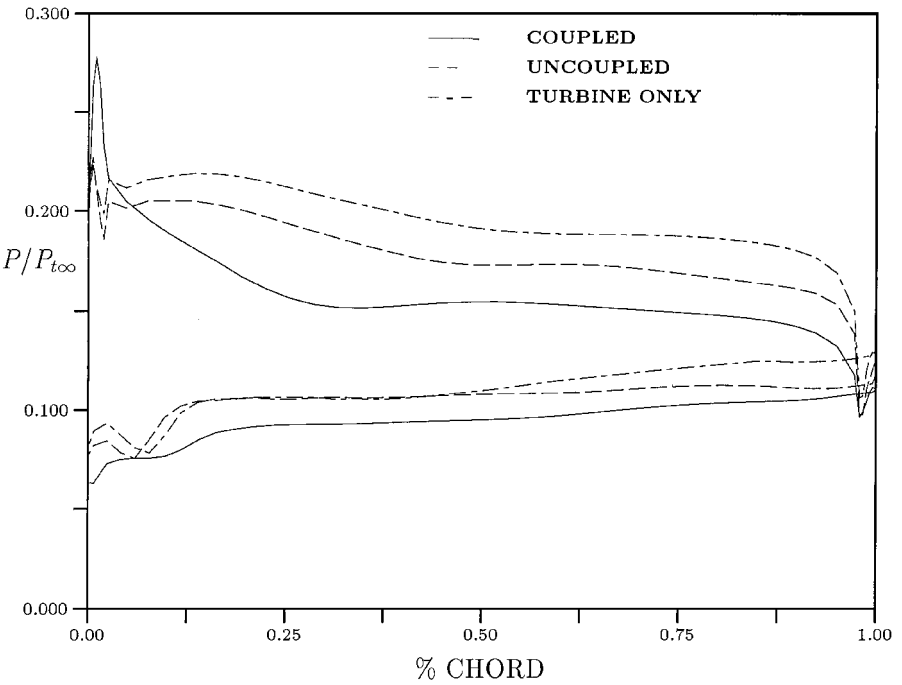

Fig. 3 Comparison of time-averaged pressure distributions, rotor midspan.

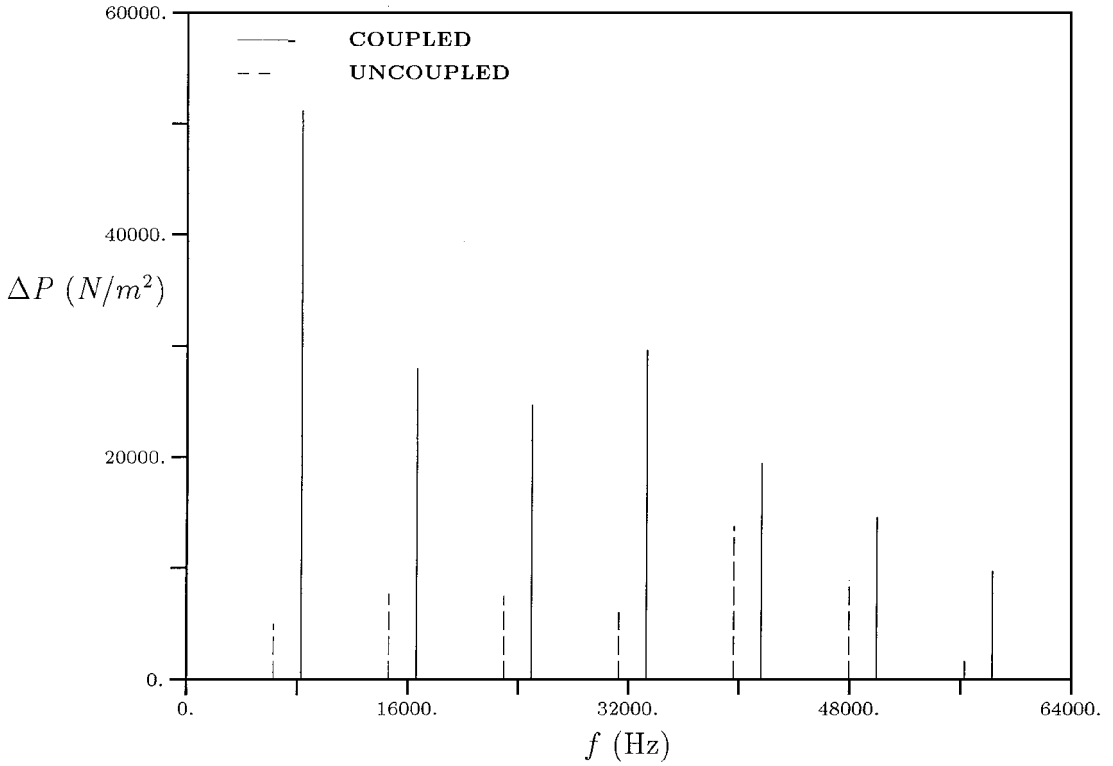

Fig. 5 Fourier decomposition of unsteady pressure, nozzle wake impact point.

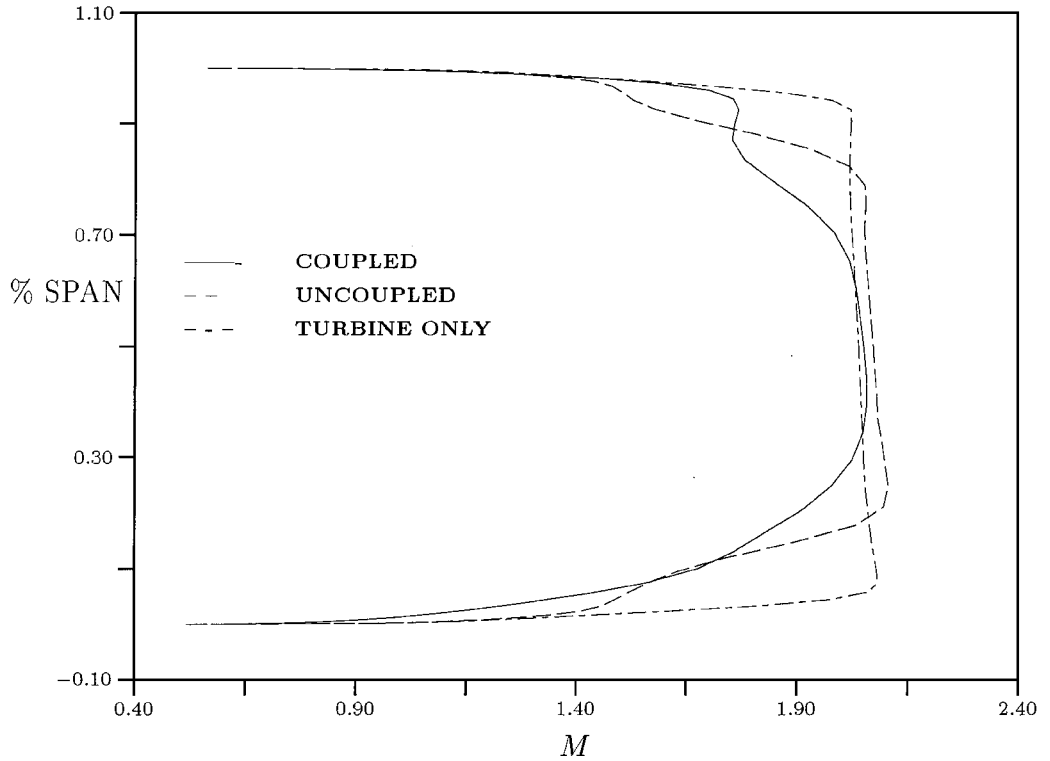

Fig. 6 Time-averaged radial profile of Mach number, rotor inlet.

and case radii at the rotor inlet were adjusted in the TA simulation to match the mass flow. The Mach number profiles at the exit of the rotor (see Fig. 7) are similar in all three simulations, with a peak Mach number of approximately $M_3 = 0.5$ at the tip and $M_3 = 0.4$ at the hub. The CO simulation, however, displays the thickest boundary layers and smoothest profile. Figure 8 contains the Mach number profiles at the exit of the EGV. The CO simulation shows the thickest endwall boundary layers, as well as the greatest peak Mach number. As suggested by Fig. 8, the flow angles in the three simulations were significantly different.

The CO simulation predicted the most work and power. The power, 869 kW, is close to target value 895 kW and has been substantiated by hot-fire tests. The power outputs in the TA (733 kW) and UN (796 kW) simulations are significantly underestimated. Because the current flow analysis has been used successfully for many interacting geometries (e.g., Refs. 1 and 4), it is assumed that the CO

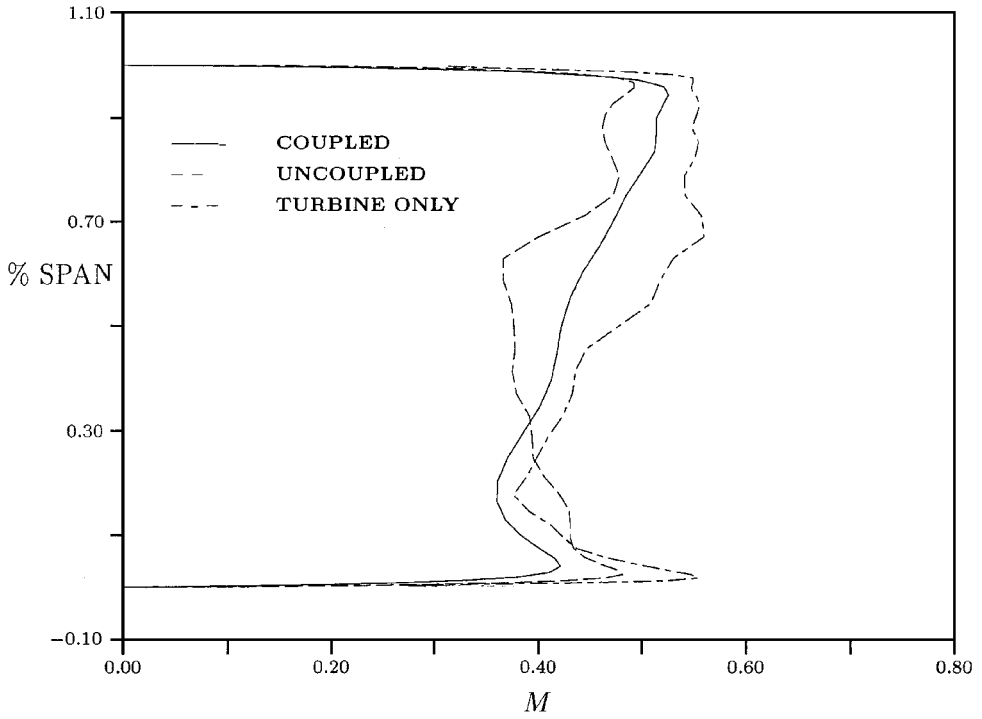

Fig. 7 Time-averaged radial profile of Mach number, rotor exit.

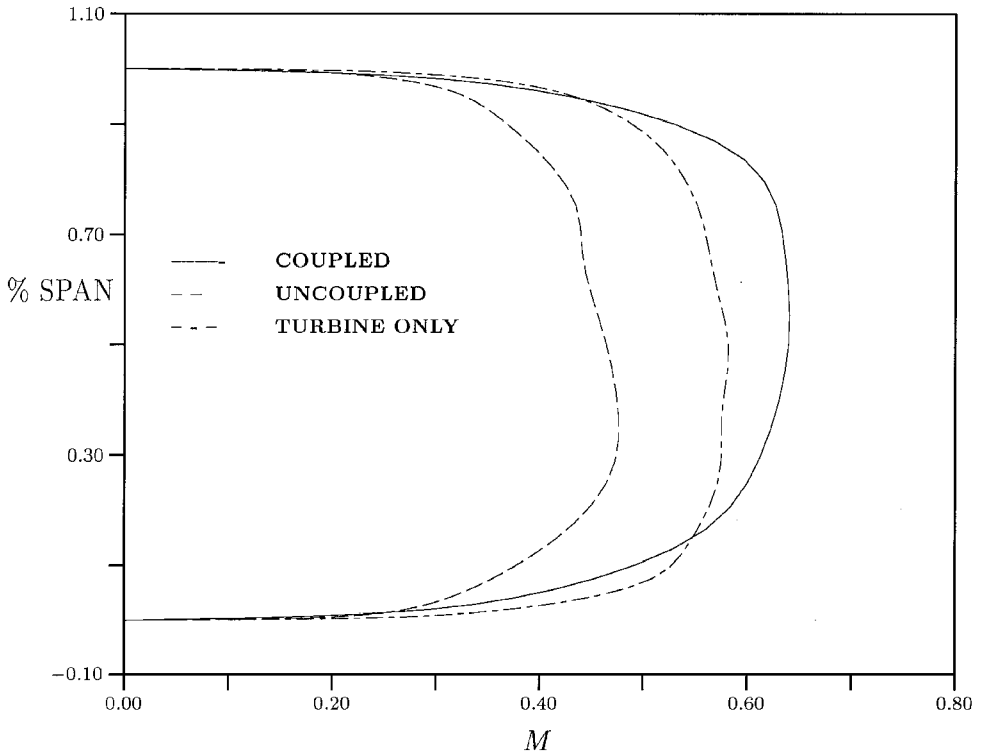

Fig. 8 Time-averaged radial profile of Mach number, EGV exit.

simulation most accurately represents the physics of the problem. The total-to-total and total-to-static efficiencies in the TA and UN simulations (62.5 and 62.8%, respectively) are greater than in the CO simulation (61.2%) because the interaction between the nozzle and rotor blades generates losses.

Conclusion

A series of numerical simulations have been performed for the Fastrac nozzle/supersonic turbine geometry. These simulations have been used to study the effects of different modeling approximations on the predicted nozzle/rotor/EGV flowfield. The results indicate that the nozzle and rotor flowfields should be coupled and solved simultaneously to predict accurately the unsteadiness generated by the nozzle/rotor interaction.

References

[1]Rangwalla, A. A., Madavan, N. K., and Johnson, P. D., "Application of an Unsteady Navier–Stokes Solver to Transonic Turbine Design," *Journal*

of Propulsion and Power, Vol. 8, No. 5, 1992, pp. 1079–1086.

[2]Griffin, L. W., and Nesman, T., "Prediction of the Unsteady Aerodymanic Environment in the RRTT Turbine," 14th Workshop for Fluid Dynamic Applications in Rocket Propulsion and Launch Vehicle Technology, NASA Marshall Space Flight Center, April 23–25, 1996.

[3]Roe, P. L., "Approximate Riemann Solvers, Parameter Vectors, and Difference Schemes," *Journal of Computational Physics*, Vol. 43, Oct. 1981, pp. 357–372.

[4]Dorney, D. J., Davis, R. L., Edwards, D. E., and Madavan, N. K., "Unsteady Analysis of Hot Streak Migration in a Turbine Stage," *Journal of Propulsion and Power*, Vol. 8, No. 2, 1992, pp. 520–529.

[5]Gundy-Burlet, K. L., "Unsteady Two- and Three-Dimensional Navier–Stokes Simulations of Multistage Turbomachinery Flows," *Journal of Computing Systems in Engineering*, Vol. 3, Nos. 1–4, 1992, pp. 231–240.

Burning Behavior of Composite Propellants with Fast-Burning Inclusions

A. E. Fogelzang,* A. P. Denisyuk,* V. V. Serushkin,†
V. Yu. Egorshev,‡ and V. P. Sinditskii§
Mendeleev University of Chemical Technology, 125047, Moscow, Russia
and
A. D. Margolin¶
Semenov Institute of Chemical Physics, 117977, Moscow, Russia

Introduction

VARIOUS applications of propellants make it necessary to modify the propellants to increase the burning rate. For the most part, this problem can be solved by the use of various combustion catalysts.[1–5] However, there comes a point where all burning rate catalyst possibilities have been exhausted, but the desired burning rate level has yet to be reached. In this case, one may employ various additives[6–8] that possess a burning rate of their own several times superior to that of the starting propellant composition. The combustion mechanism of such compositions has not been fully considered, though an increase in the burning rate was assumed to be due to a cratering effect in the burning propellant caused by extremely fast decomposition of particles of the additive.[6] Thus far it is not clear, however, how the particle size, burning rate, and content of additive entered into a propellant composition can influence the burning rate and character of $r_b(p)$ dependence. In this connection, the effect on the burning rate of entering fast-burning energetic materials (FBEM) into ammonium perchlorate–polymeric binder propellant formulations has been studied.

Experimental

Lead salt of 2,4,6-trinitro-meta-cresol (LTNC), the combustion of which has been studied previously,[9] was used as the fast-burning additive. It is a stable compound with ignition temperature of 250 K and demonstrates a burning rate 21.6 cm/s at 10 MPa, that is, almost 10 times faster than conventional composite propellants. Grains of LTNC were prepared by granulating tablets of the substance pressed at 500 MPa to the density of 2.34 g/cm^3 followed by sieving.

A window constant-pressure bomb of 1.5-liter volume pressurized with nitrogen was used to measure the burning rate of compositions in the pressure range 0.1–40 MPa. The behavior and velocity of burning were registered using a slit camera. In preparing the strands, uncured propellant compositions containing LTNC grains were put into transparent acrylic tubes 7 or 12 mm i.d. and 30–50 mm height.

The delay time of ignition of the propellant layer immediately under an FBEM grain was determined using strands separated into two parts with a pressed FBEM tablet approximately 1 mm thick and 7 mm diameter. The slit camera was used to record the front of flame propagation through the propellant-FBEM tablet-propellant strand section that allowed the delay of ignition of the lower propellant layer to be derived from the record.

Results and Discussion

Incorporation of LTNC of fine particle size (less than 10 μm) into propellant, which burnt at 2.2 cm/s at 10 MPa, failed to enhance the burning rate (Fig. 1). Quite different observations have been made when the FBEM particle size was changed. Figure 1 shows that an increase in the LTNC particle size to 500 μm lead to a progressive enhancement of the burning rate of the propellant composition containing 15% LTNC grains. On further increasing the particle size, the burning rate of the composition remained practically unchanged.

Previous experiments on critical combustion diameter d_c showed that d_c of LTNC was equal to 15 μm, and there was no change in the LTNC burning rate within the 100–1000 μm diameter range. It follows, therefore, that the observed decrease in the composition burning rate as LTNC particle size decreases from 500 to 100 μm (see Fig. 1) cannot be attributed to the influence of the critical combustion diameter.

To explain the results observed, let us consider a simple combustion model of a propellant formulation containing FBEM grains. The FBEM grains are assumed to be of spherical form, to have diameter d, to have the burning rate of their own r_{FBEM} superior to that of the baseline propellant, and to be evenly distributed in the propellant bulk, as shown in Fig. 2. In the case of the one-dimensional model, the time of combustion of a unit volume is a sum of combustion times of the propellant layers above and under an FBEM particle and the particle itself. Also one may suggest the occurrence of some delay in ignition of the propellant layer underneath the FBEM particle due

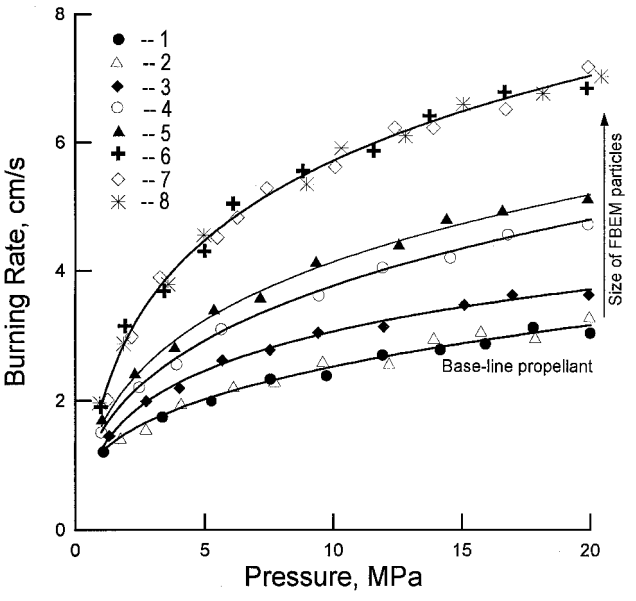

Fig. 1 Burning rate vs pressure for a composite propellant containing 15% LTNC grains at different LTNC particle sizes: 1, baseline propellent; 2, less than 10 θm; 3, less than 100 θm; 4, 200–315 θm; 5, 315–400 θm; 6, 400–630 θm; 7, 630–800 θm; and 8, 800–1000 θm.

Received 4 March 1999; revision received 27 October 1999; accepted for publication 2 November 1999.

*Professor, Department of Chemical Engineering, 9 Miusskaya Square; vvs@rctu.ru.

†Associate Professor, Department of Chemical Engineering, 9 Miusskaya Square; vvs@rctu.ru.

‡Senior Scientist, Department of Chemical Engineering, 9 Miusskaya Square.

§Associate Professor, Department of Chemical Engineering, 9 Miusskaya Square; vps@rctu.ru.

¶Professor, 4 Kosygin Street.